International Journal of Minerals, Metallurgy and Materials
Volume 23, Number 1, January 2016, Page 49
DOI: 10.1007/s12613-016-1210-7

Effects of simulated on-fire processing conditions on the microstructure and mechanical performance of Q345R steel

Yi-chao Peng[1)], *Hao-hao Xu*[1)], *and Mai-cang Zhang*[2)]

1) Department of Materials Technology, Zhejiang Energy Technology & Research Co. Ltd., Hangzhou 310003, China
2) Department of Materials Science and Engineering, University of Science and Technology Beijing, Beijing 100083, China
(Received: 10 May 2015; revised: 9 August 2015; accepted: 1 September 2015)

Abstract: A series of simulated on-fire processing experiments on Q345R steel plates was conducted, and the plates' Brinell hardness, tensile strength, and impact energy were tested. Microstructure morphologies were systematically analyzed using a scanning electron microscope with the aim of investigating the effect of the steel's microstructure on its performance. All examined performance parameters exhibited a substantial decrease in the cases of samples heat-treated at temperatures near 700°C. However, although the banded structure decreased with increasing treatment temperature and holding time, it had little effect on the performance decline in fact. Further analysis revealed that pearlite degeneration near 700°C, which was induced by the interaction of both subcritical annealing and conventional spherical annealing, was the primary reason for the degradation behavior. Consequently, some nonlinear mathematical models of different mechanical performances were established to facilitate processing adjustments.

Keywords: low alloy steels; heat treatment; mechanical properties; microstructure; nonlinear mathematical models

1. Introduction

Q345R steel has been widely used to manufacture pressure vessels [1]. As Q345R steel is a low-alloy structural steel, it must exhibit excellent mechanical performance to satisfy practical requirements for such applications. Therefore, much attention has been devoted to improve the mechanical properties of Q345R steel without substantially increasing its cost [2–4]. In recent years, the effects of trace elements (e.g., V, Nb, and Al) [5] and cooling rate during processing [6] have been extensively investigated. Zhao [7] studied the relation between different rolling processes and the microstructure and properties of the resulting steel. However, the influence of microstructure on the steel's mechanical performance and the corresponding relation equations remain unsolved issues. In the case of Q345R, a banded structure that contains alternating ferrite and pearlite bands is commonly observed [8]. This banded structure usually forms during the austenite-to-ferrite transformation when the as-rolled steel plates are gradually cooled [9]. Actually, the formation mechanism is related to the original segregation of substitutional alloying elements into the liquid phase during dendritic solidification [9–10]. However, eliminating these bands through long-term, high-temperature homogenization is difficult because of the low diffusion rates of the substitutional elements [11]; consequently, heat treatments are not economically feasible. Furthermore, another important phenomenon known as pearlite degeneration has also aroused researchers' interest. The typical characteristic of pearlite degeneration is the spheroidization of cementite [12]. Studies on the static spheroidization of silicon-containing steel have shown that the spheroidization rate is controlled by the diffusion of carbon at the Fe–Fe_3C interface [13]. Generally, subcritical annealing and intercritical annealing would result in such a transformation [14].

Because the service states of Q345R steel plates are strongly affected by their processing conditions, a systematic analysis of the effects of processing conditions is important. In this study, a series of on-fire processing experiments was conducted to study the influence of processing conditions and the mechanism of performance degradation. Furthermore, nonlinear mathematical models of the relevant

Corresponding author: Yi-chao Peng E-mail: peng3383118@163.com

relations were established to facilitate the development of production technologies.

2. Material and methods

The material studied in this paper was as-rolled Q345R steel. The chemical composition (wt%) was C, ≤0.20; Si, ≤0.55; Mn, 1.20–1.60; P, ≤0.025; S, ≤0.015; Al_t, ≥0.02; Fe, balance. In the experiments, the steel plates were first machined to dimensions of 200 mm × 200 mm × 20 mm and then heat-treated isothermally in an SX-5-10 resistance furnace (Shanghai Shuli Instrument Co., Ltd.) at 550, 700, 800, and 950°C for 0.5 h, 2 h, and 5 h at each temperature, followed by being cooled in air.

Several mechanical tests were conducted after the aforementioned heat treatment to reveal the variation in performance with variation of the heat-treatment parameters. The surface hardness was tested using an XHB-3000 Brinell hardness tester. Tensile tests and Charpy V-notch impact tests were subsequently performed at room temperature using MTS-800 (Mechanical Testing and Sensing Systems Corporation) and JB-W (Beijing Time High Technology Co., Ltd.) testing machines, respectively.

Specimens with dimensions of 10 mm × 10 mm × 20 mm for microstructure analysis were cut from the bulk processed steel plates. The microstructure morphologies were observed using a 9XB-PC optical microscope (Shanghai Optical Instrument Factory) and a JSM-6510A scanning electron microscope (Japan Electron Optics Laboratory Co., Ltd.).

3. Results and discussions

3.1. Mechanical properties of Q345R steel

Fig. 1 shows the variation trends of Brinell hardness (HB), impact energy (A_k), and tensile strength (R_m) as functions of heat-treatment temperature. As evident in the figure, most of the curves exhibit a similar trend, i.e., the curves remain relatively stable for treatment temperatures from room temperature to 550°C, decrease sharply for treatment temperatures between 550°C and 700°C, and again increase when the treatment temperature exceeds 700°C. The mechanical performance of the steel samples treated under the corresponding conditions depends primarily on temperature and weakly on the holding time. Therefore, given the economic feasibility and safety requirements, the processing temperatures should avoid close to 700°C and the holding time should be as short as possible while maintaining the predominant properties of the steel.

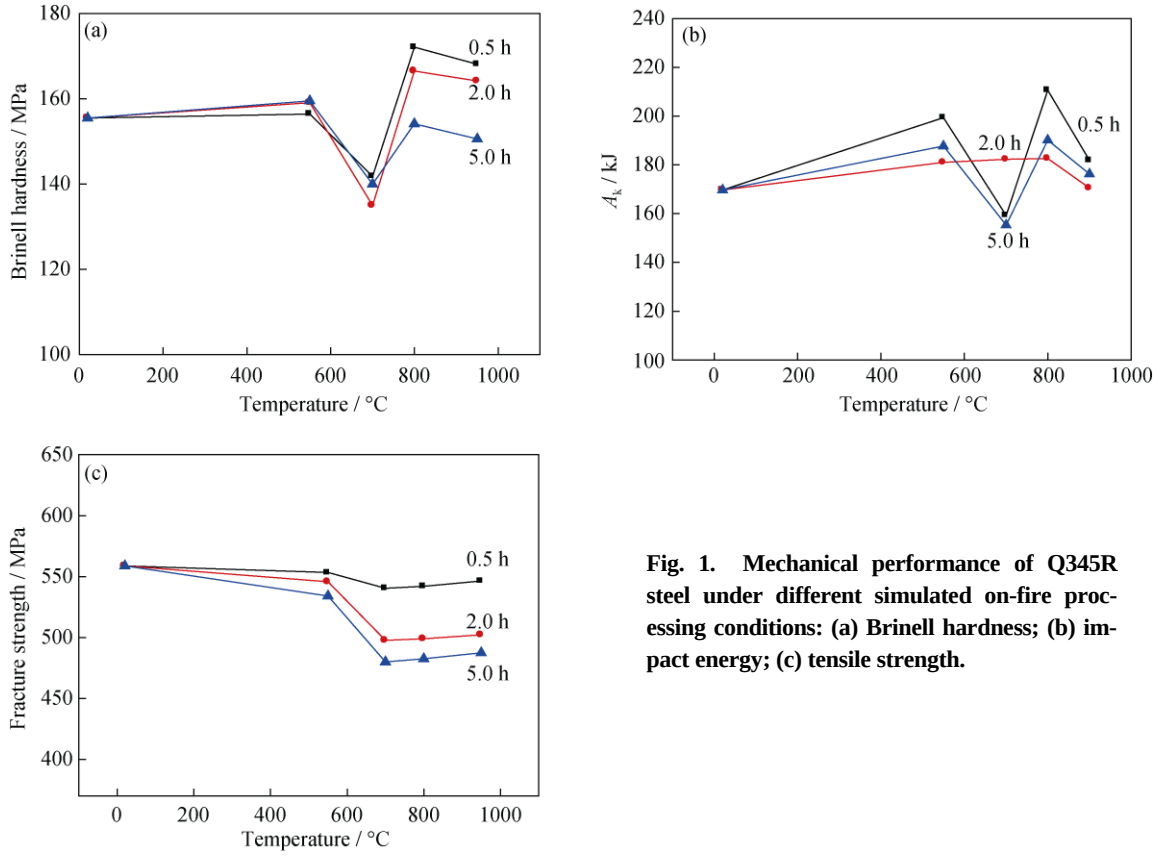

Fig. 1. Mechanical performance of Q345R steel under different simulated on-fire processing conditions: (a) Brinell hardness; (b) impact energy; (c) tensile strength.

Notably, the processing conditions used in this work are focused primarily on the influence of heat treatments. Other factors, such as the load on the plates and surface oxidation, are not considered.

3.2. Microstructure of Q345R

3.2.1. Banded structure of Q345R

Fig. 2 reveals the metallographic characteristics of Q345R steel. The banded feature is obvious, especially under the conditions of low temperature or inadequate treatment time. In the images, the dark and white zones are pearlite and ferrite, respectively. In accordance with Chinese standard GB/T 13299—1991 "Microstructure assessment methods of steels", the banded levels were measured under different conditions; the results are reported in Table 1. The levels clearly remain stable from 550°C to 700°C and then begin to decrease at higher treatment temperatures and longer treatment time. In the case of the sample treated at 950°C for 5 h, the banded structure level is only approximately 1B; i.e., the pearlite and ferrite are evenly distributed. As shown in Fig. 2, elimination of these bands requires a higher temperature and an adequate holding time.

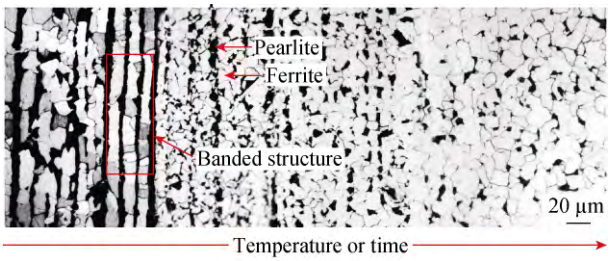

Fig. 2. Variation of the banded structure with processing conditions (temperature or time).

Table 1. Banded levels of the tested specimens in different states

Time / h	550°C	700°C	800°C	950°C
0.5	4B	4B	4B	3.5B
2	4B	4B	3B	1.5B
5	4B	4B	2B	1B

The banded structure originates from original heterogeneous segregation of alloy elements during dendritic solidification. Because of the relatively high Mn and Si contents, dendritic segregation is prone to occur during the solidification process; i.e., alloy elements are inclined to segregate to interdendritic sites. However, in the subsequent hot-forming process, a homogeneous state is difficult to achieve through diffusion because of the low diffusion coefficient of Mn. Thus, a certain degree of banded segregation will continue to exist. The formation mechanism of the banded structure can be interpreted through the diffusion behaviors of C, Mn, and Si in the Fe matrix. As presented in Fig. 3, the distribution of alloy elements over a wide range appears as an undulating curve. The peaks of this curve indicate a greater content of Mn, thus leading to undulating distributions of the A_{r3} temperature among different regions. During the cooling process, ferrite first forms in bands with a high A_{r3} temperature and carbon is forced into the adjacent low-A_{r3} austenite because of the low solubility of carbon in ferrite; these processes lead to the formation of carbon-rich and carbon-depleted layers [15]. The carbon concentration gradually increases at the segregation region of the alloy elements, and austenite in these carbon-rich or Mn- rich regions finally transforms into pearlite or proeutectoid ferrite and pearlite, resulting in a banded distribution of ferrite and pearlite. However, at higher on-fire temperatures such as 800°C or 950°C, the microstructure undergoes considerable changes, as shown in Fig. 4; i.e., the bands decrease or even disappear but the performance of the steel changes little. Thus, the performance of Q345R steel is not sensitive to ferrite and pearlite existing in a banded distribution. In fact, certain mechanical properties such as tensile strength, yield strength, or elongation are not substantially affected by microstructural banding, primarily because the direction of the main working force of a pressure vessel is the rolling or transversal direction, allowing the anisotropic effects in the thickness direction to be ignored.

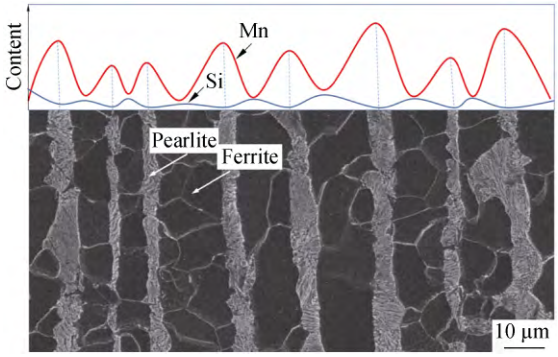

Fig. 3. Schematic of Mn segregation and the corresponding banded structure.

3.2.2. Degeneration of pearlite

The most significant feature for Q345R treated at 700°C is pearlite degeneration. The typical characteristics are the breakup of lamellar cementites and spheroidization of cementite particles, as shown in Fig. 5. This figure shows chains of discrete, broken-up cementite in the sample treated at 700°C for 0.5 h, rod-shaped structures in the sample treated at 700°C for 2 h, and a series of spheres or approximately spherical particles in the sample treated at 700°C for 5 h. Thus, pearlite degeneration tends to increase with increasing treatment time.

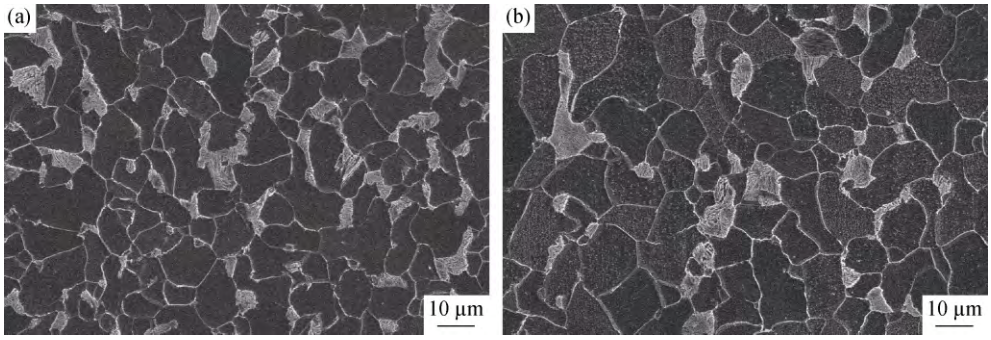

Fig. 4. Microstructures of Q345R steel heat-treated at 950°C for 2 h (a) and 5 h (b).

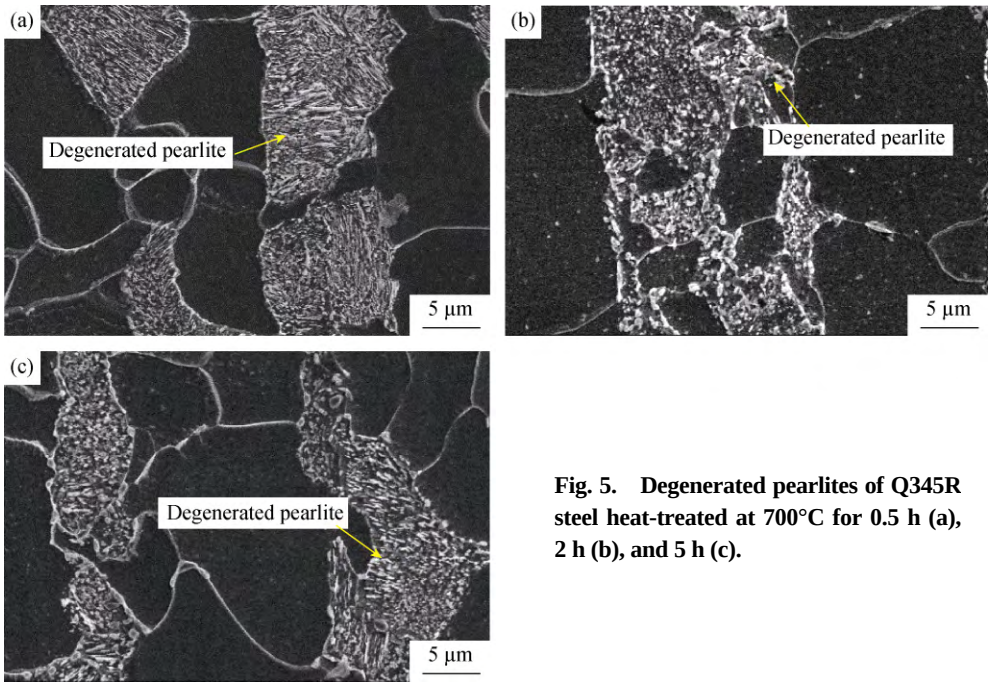

Fig. 5. Degenerated pearlites of Q345R steel heat-treated at 700°C for 0.5 h (a), 2 h (b), and 5 h (c).

The CCT (continuous cooling transformation) curves of Q345R were calculated using the Jmat-Pro software on the basis of the Fe-based data in its database; the results are plotted in Fig. 6. The calculated curves indicate that the values of A_1 and A_3 approach 701.2°C and 828.3°C, respectively.

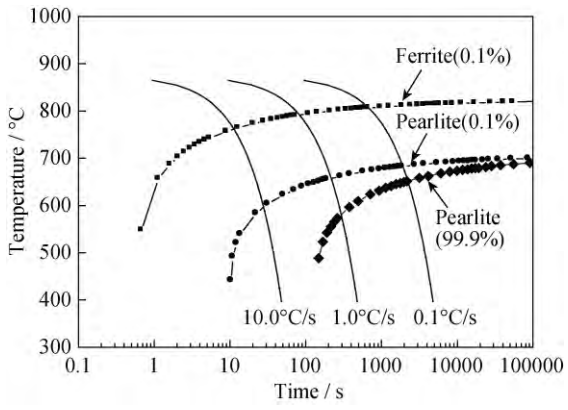

Fig. 6. CCT diagram for Q345R steel.

Several models have been proposed to explain the mechanism of spheroidization of lamellar cementites, including capillarity-induced perturbation theory, grain-boundary thermal groove theory, and fault migration theory [16]. In the case of the as-rolled Q345R steel plates, high-density dislocations exist in the pearlite. After gaining sufficient activation energy during high-temperature recovery, slip dislocations in cementite will climb directly, leading to rearrangement or cancelation of different kinds of dislocations and subsequent formation of subgrains. A sub-boundary groove due to local equilibrium of surface tension introduces curvature to the lamellar cementites at the interface, thus causing a distinction of curvature between grooves and neighboring flat interfaces [16]. Because the saturated concentration, as indicated by the Gibbs–Thomson effect, increases with increasing curvature of the surface of cementites, it will result in a concentration gradient between the two sites. The mathematical formula for the Gibbs–Thomson effect is given as follows:

$$C_r^{\alpha} = C_{\infty}^{\alpha}\left[1+\frac{2\sigma V}{RT}\cdot\frac{1}{r}\right] \quad (1)$$

where r is the radius of curvature and C_{∞}^{α} is the saturated concentration when r tends to infinity. In response to the concentration gradient, carbon dissolved in α-solution at the grooves will spread to the adjacent flat, gradually leading to dissolution of the groove and eventually to break-up of the lamellar plates. Ostwald ripening, i.e., the growth of larger particles and dissolution of smaller particles, then occurs. The whole aforementioned process results in the degeneration of pearlite, as demonstrated in Fig. 7. Tian and Kraft [17] have summarized the main points of these models on the basis of their experimental results, which showed that the recession of lamellar terminations, expansion of holes, growth of fissures, and the thickening of lamellae together contribute to the final shape of the degenerated pearlite. At a treatment temperature of 700°C, the rate of the spheroidization process increases with time because of the sufficient dissolution of terminations and the rapid diffusion of carbon. A high degree of degeneration is therefore achieved.

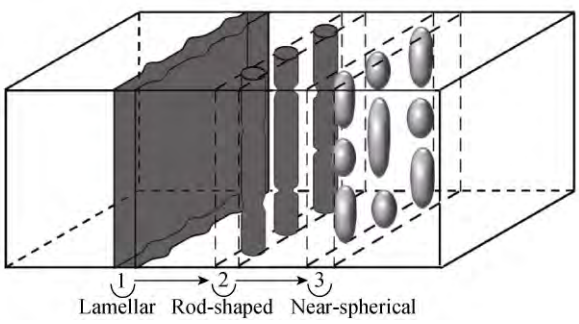

Fig. 7. Schematic illustrating the degeneration of pearlite during subcritical annealing.

Given that 700°C is in the range of the critical fluctuation around the A_{r1} temperature of Q345R, the process of conventional spheroidization should not be ignored. Fig. 8 illustrates the difference between the two spheroidization processes. In conventional spheroidization annealing, insufficient austenitization always results in certain number of undissolved carbide particles remaining in austenite at temperatures above the A_1 temperature. In addition, in the subsequent slow-cooling stage at temperatures below A_1, these particles become cementite nuclei, resulting in the formation of final spherical carbides [18]. O'Brien and Hosford [14] concluded that the subcritical process requires substantially less time for spheroidization than the conventional process and will greatly reduce energy consumption if adopted.

The ability of spheroidal carbides to block dislocation movement is less than that of lamellar carbides. Thus, dislocations will pile up at the interface of lamellar carbides and must achieve a greater force or activation energy to overcome this block. However, dislocations in the face of spheroidal carbide particles can bypass such blocks and continue to migrate. The strengthening effect is diminished because of the decrease in phase boundaries or increase in the degree of spheroidization.

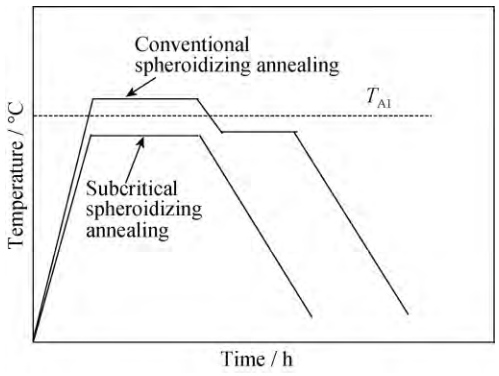

Fig. 8. Comparison between conventional and subcritical spheroidization annealing.

3.3. Nonlinear mathematical modeling

3.3.1. Basic principle of the nonlinear regression method

The nonlinear regression model is shown as follows:

$$\boldsymbol{y} = f(\boldsymbol{\xi},\boldsymbol{\theta}) + \boldsymbol{\omega} \quad (2)$$

where $\boldsymbol{y}$ is a dependent variable; $\boldsymbol{\xi} = [\xi_1, \xi_2, \cdots, \xi_k]^{\mathrm{T}}$ is a vector composed of k independent variables; $\boldsymbol{\theta} = [\theta_1, \theta_2, \cdots, \theta_p]^{\mathrm{T}}$ is a vector composed of p undetermined parameters; and $\boldsymbol{\omega}$ is the deviation of random variables following a normal distribution.

Assume that n groups of independent observed values exist: $(\boldsymbol{\xi}_i, \boldsymbol{y}_{ie})$, $i = 1, 2, \cdots, n$, where $\boldsymbol{\xi}_i = [\xi_{1i}, \xi_{2i}, \cdots, \xi_{ki}]^{\mathrm{T}}$ and $\boldsymbol{y}_{ie}$ are the observed values corresponding to $\boldsymbol{\xi}_i$. According to the principle of least squares, $\hat{\boldsymbol{\theta}}$, the optimal estimation of $\boldsymbol{\theta}$, can be determined optimally using the following objective function:

$$\boldsymbol{S}(\hat{\boldsymbol{\theta}}) = \min \boldsymbol{S}(\boldsymbol{\theta}) = \min \sum_{i=1}^{n} (\boldsymbol{y}_{ie} - \boldsymbol{y}_i)^2 \quad (3)$$

where $\boldsymbol{y}_i = f(\boldsymbol{\xi}_i, \boldsymbol{\theta})$.

Because of the nonlinearity of the regression model, the optimization problem turns to solving the nonlinear equations formed by $\boldsymbol{G}(\boldsymbol{\theta}) = \boldsymbol{0}$, the gradient of $\boldsymbol{S}(\boldsymbol{\theta})$. Solving these nonlinear equations directly is difficult. In reference to the Gauss–Newton method and Marquardt method, we adopted the Newton–Raphson iteration method to solve the equations after linearization of the objective function.

Assuming that the m–1-th result of the iteration and the correction amount are $\boldsymbol{\theta}^{m-1}$ and $\boldsymbol{\beta}^m$, respectively, the m-th iteration result can be determined using the following formula:

$$\boldsymbol{\theta}^m = \boldsymbol{\theta}^{m-1} + \boldsymbol{\beta}^m \quad (4)$$

Substituting Eq. (4) into Eq. (3) and then conducting the

Taylor expansion at $\boldsymbol{\theta}^{m-1}$ to take its linear term, we obtain the following equation:

$$\min \boldsymbol{S}(\boldsymbol{\theta}) = \min \sum_{i=1}^{n} \left[\boldsymbol{y}_{ie} - f(\boldsymbol{\xi}_i, \boldsymbol{\theta}^{m-1}) - \left(\sum_{j=1}^{p} \frac{\partial f(\boldsymbol{\xi}_i, \boldsymbol{\theta}^{m-1})}{\partial \boldsymbol{\theta}_j} \right) \boldsymbol{\beta}^m \right]^2 \quad (5)$$

Let $\boldsymbol{B}$ be an n-dimensional column vector whose components are $\boldsymbol{B}_{ij} = \boldsymbol{y}_{ie} - f(\boldsymbol{\xi}_i, \boldsymbol{\theta}^{m-1})$. Likewise, let $\boldsymbol{A}$ be an $n \times p$ matrix whose components are $\boldsymbol{A}_{ij} = \sum_{j=1}^{p} \left[\partial f(\boldsymbol{\xi}_i, \boldsymbol{\theta}^{m-1}) / \partial \boldsymbol{\theta}_j \right]$, where $i = 1, 2, \cdots, n$; $j = 1, 2, \cdots, p$. Thus, the equations composed of gradient $\boldsymbol{G}(\boldsymbol{\theta}) = \boldsymbol{0}$ of Eq. (5) can be written as

$$\boldsymbol{A}\boldsymbol{\beta} = \boldsymbol{B} \quad (6)$$

The value of correction is obtained by solving Eq. (6).

3.3.2. Nonlinear mathematical model for the properties of Q345R treated at different temperatures

To predict relevant mechanical properties under other conditions for later production reference, we attempted to establish nonlinear mathematical models for these properties. Notably, because the influence of treatment time on the Brinell hardness is relatively weak, only on-fire temperature is considered here. A nonlinear model is given as follows when t is constant:

$$\mathrm{HB}(T) = f(T) = p_1 + \frac{p_2}{p_3 + \exp(T/1000)^m}, \; t = \text{const} \quad (7)$$

where HB is the Brinell hardness, T is the experimental temperature, and p_1, p_2, p_3, and m are undetermined parameters. Using the least-squares principle, we fitted the experimental data nonlinearly and optimized the fit through the Levenberg–Marquardt (LM) method. The undetermined parameters for different treatment time were then optimally estimated; the results are reported in Table 2. Notably, to increase the number of samples, we conducted a linear interpolation between experimental values obtained for samples treated for 2 and 5 h to obtain another value for a sample treated for 3.5 h. The HB curve for Q345R based on this mathematical model is presented in Fig. 9.

Table 2. Undetermined parameters of the nonlinear model for Brinell hardness

Holding time / h	p_1	p_2	p_3	m
0.5	162.8	0.145	–1.018	12.400
2	160.4	0.159	–1.032	10.310
3.5	155.8	–0.00669	–2.722	–0.0041
5	154.9	–0.00608	–2.726	–0.0082

Fig. 10 shows a comparison between the calculated data obtained from the nonlinear mathematical model and experimental HB data for different heat-treatment holding time. The results show that the fitted curves reflect the basic trend of the experimental data. In addition, the maximum relative error (Max RE) between them is less than 4%, fully demonstrating that the prediction accuracy of the model satisfies the engineering requirements.

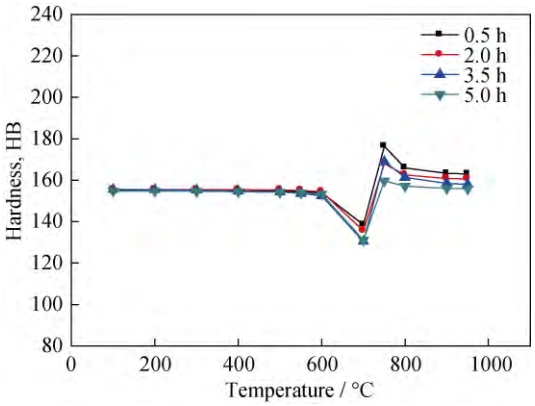

Fig. 9. HB curves of Q345R based on the mathematical model.

The aforementioned nonlinear model was further applied to fit the tensile strength and impact energy. Eqs. (8) and (9) show the fitting relations between the treatment temperature and the tensile strength and impact energy, respectively.

$$R_{\mathrm{m}}(T) = 553.358 + \frac{273.381}{\exp\left(\frac{T}{1000}\right)^{-2.851} - 36.028} \quad (8)$$

$$A_{\mathrm{k}}(T) = 172.432 + \frac{-37.512}{\exp\left(\frac{T}{1000}\right)^{-2.381} - 6.482} \quad (9)$$

Fig. 11 shows a comparison between the calculated and tested values of tensile strength and impact energy for Q345R plates thermally treated for 0.5 h. Because relatively few test points are available, the fitting curves obtained by the models do not exactly match the experimental data. However, the Max REs between the fitting points and the experimental points are still less than 4%. Therefore, these nonlinear models provide some correlation to practical applications.

The previously discussed mathematical modeling demonstrates the applicability of nonlinear regression to numerical simulation and further optimization. The choice of a suitable model, such as the Levenberg–Marquardt method employed here, can greatly improve the convergence precision and rate of the iterative.

4. Conclusions

(1) Elimination of the banded structure by diffusion in Q345R steel plates requires a high temperature and sufficient holding time. However, the elimination of the banded structure has little effect on performance degradation in cases where the heat treatment temperature is approximately 700°C.

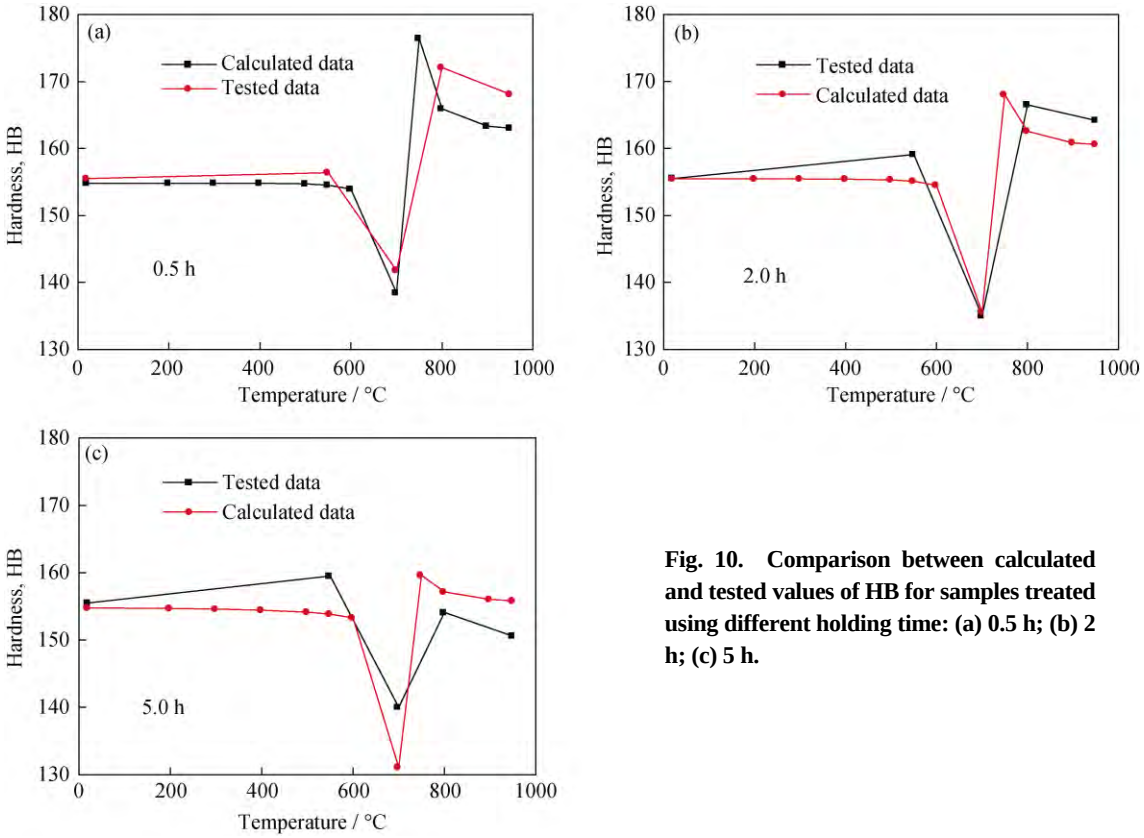

Fig. 10. Comparison between calculated and tested values of HB for samples treated using different holding time: (a) 0.5 h; (b) 2 h; (c) 5 h.

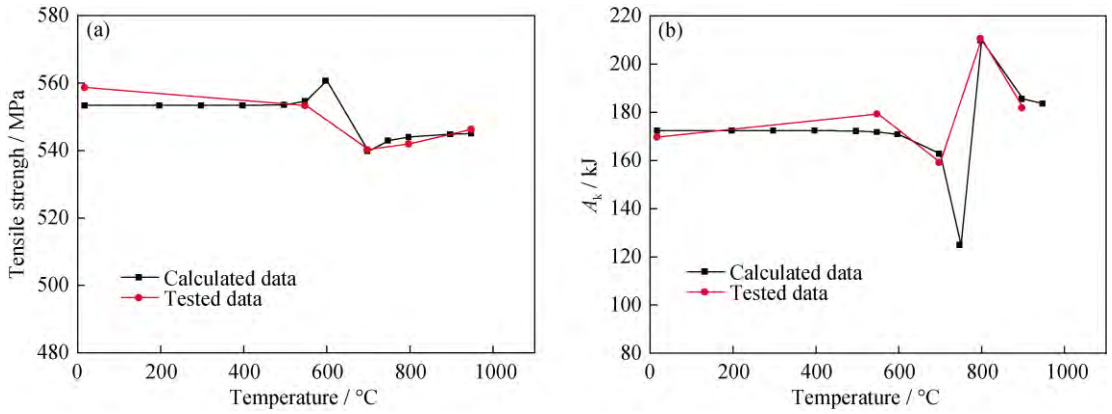

Fig. 11. Comparison between calculated and tested values of tensile strength (a) and impact energy (b) for Q345R steel plates heat-treated for 0.5 h.

(2) The annealing temperature for processing should be substantially greater or substantially lower than 700°C to prevent the sharp decrease of many properties that occurs near this temperature. Further, pearlite degeneration, which leads to diminished performance of the steel, also occurs near 700°C. The results reveal that the subcritical spheroidization annealing and conventional spheroidization annealing may together contribute to the degeneration of pearlite.

(3) Some nonlinear mathematical models of different mechanical properties were established to predict the relevant performance of Q345R steel under other conditions encountered in practical applications.

Acknowledgements

The author is grateful for the financial support and facilities provided by the China Special Equipment Inspection and Research Institute and by the State Key Laboratory for Advanced Metals and Materials, respectively.

References

[1] P.J. Guo, X.D. Chen, W.H. Guan, H.Y. Cheng, and H. Jiang, Effect of tensile stress on the variation of magnetic field of low-alloy steel, *J. Magn. Magn. Mater.*, 323(2011), No. 20, p. 2474.

[2] Y. Yan, A.Z. Liu, and D.X. Zhou, Research on mechanical properties of 16MnR steel after high temperature damage, *J. Hefei Univ. Technol. Nat. Sci.*, 34(2011), No. 6, p. 827.

[3] A.Z. Liu and S. Zhang, Relationships between fatigue mechanical properties and roughness of fatigue fracture about 16MnR steel after high temperature, *Adv. Mater. Res.*, 602-604(2013), p. 333.

[4] Z.C. Fan and J.L. Jiang, Investigation of low cycle fatigue behavior of 16Mn R steel at elevated temperature, *J. Zhejiang Univ. Eng. Sci.*, 38(2004), No. 9, p. 1190.

[5] S.X. Liu, Y. Chen, Z.Y. Zhao, R.D. Xue, X.E. Li, and J.H. Fan, Effect of microalloy element on the grain coarsening behavior of Q345 steel, *Foundry Technol.*, 27(2006), No. 10, p. 1071.

[6] S. Shanmugam, N. Ramisetti, R.D.K. Misra, T. Mannering, D. Panda, and S. Jansto, Effect of cooling rate on the microstructure and mechanical properties of Nb-microalloyed steels, *Mater. Sci. Eng. A*, 460-461(2007), p. 335.

[7] L. Zhao, Research and analysis on properties of Q345R vessel steel, *Phys. Exam. Test.*, 30(2012), No. 1, p. 5.

[8] F.A. Khalid, M. Farooque, A. ul Haq, and A.Q. Khan, Role of ferrite/pearlite banded structure and segregation on mechanical properties of microalloyed hot rolled steel, *Mater. Sci. Technol.*, 15(1999), No. 10, p. 1209.

[9] A. Karma and A. Sarkissian, Dynamics of banded structure formation in rapid solidification, *Phys. Rev. Lett.*, 68(1992), No. 17, p. 2616.

[10] J.D. Verhoeven, A review of microsegregation induced banding phenomena in steels, *J. Mater. Eng. Perform.*, 9(2000), No. 3, p. 286.

[11] X.Z. Li, J.J. Guo, Y.Q. Su, S.P. Wu, and H.Z. Fu, Formation mechanism of band structure and phase selection during directional solidification of peritectic alloys I: formation mechanism of band structure, *Acta Metall. Sin.*, 41(2005), No. 6, p. 593.

[12] Y.H. Su, S. Morooka, M. Ohnuma, J. Suzuki, and Y. Tomota, Quantitative analysis of cementite spheroidization in pearlite by small-angle neutron scattering, *Metall. Mater. Trans. A*, 46(2015), No. 4, p. 1731.

[13] G.H. Zhang, D.W. Suh, and K.M. Wu, Effects of Mn, Si and Cr addition on the spheroidization of cementite in hypereutectoid Fe-1mass%C steel, *Mater. Sci. Forum*, 783-786(2014), p. 1053.

[14] J.M. O'Brien and W.F. Hosford, Spheroidization cycles for medium carbon steels, *Metall. Mater. Trans.*, 33(2002), No. 4, p. 1255.

[15] T.F. Majka, D.K. Matlock, and G. Krauss, Development of microstructural banding in low-alloy steel with simulated Mn segregation, *Metall. Mater. Trans. A*, 33(2002), No. 6, p. 1627.

[16] Y.T. Wang, Y. Adachi, K. Nakajima, and Y. Sugimoto, Quantitative three-dimensional characterization of pearlite spheroidization, *Acta Mater.*, 58(2010), No. 14, p. 4849.

[17] Y.L. Tian and R.W. Kraft, Mechanisms of pearlite spheroidization, *Metall. Trans. A*, 18(1987), No. 8, p.1403.

[18] S.C. Wang and P.W. Kao, The effect of alloying elements on the structure and mechanical properties of ultra low carbon bainitic steels, *J. Mater. Sci.*, 28(1993), No. 19, p. 5169.